1   **Investigating the Impact of Aerosol Deposition on Snow**

2   **Melt over the Greenland Ice Sheet Using a Large-Ensemble**

3   **Kernel**

4   Yang Li[1], Mark G. Flanner[1]

5   [1] Climate and Space Sciences and Engineering, University of Michigan, Ann Arbor, Michigan, USA

6

7   **Correspondence to:** Y. Li, yanglibj@umich.edu

8

9   **Abstract**

10   Accelerating surface melt on the Greenland Ice Sheet (GrIS) has led to a doubling of

11   Greenland's contribution to global sea level rise during recent decades. Black

12   carbon (BC), dust, and other light absorbing impurities (LAI) darken the surface and

13   enhance snow melt by boosting the absorption of solar energy. It is therefore

14   important for coupled aerosol-climate and ice sheet models to include snow

15   darkening effects from LAI, and yet most do not. In this study, we conduct several

16   thousand simulations with the Community Land Model (CLM) component of the

17   Community Earth System Model (CESM) to characterize changes in melt runoff due

18   to variations in the amount, timing, and nature (wet or dry) of BC deposition on the

19   GrIS. From this large matrix of simulations, we develop a kernel relating runoff to

20   the location, month, year (from 2006-2015), and magnitudes of BC concentration

21   within precipitation and dry deposition flux. BC deposition during June-August

22   causes the largest increase in annually-integrated runoff, but winter deposition

23   events also exert large (roughly half as great) runoff perturbations due to re-

24   exposure of impurities at the snow surface during summer melt. Current BC

25   deposition fluxes simulated with the atmosphere component of CESM induce a

26   climatological-mean increase in GrIS-wide runoff of ~8 Gt/yr, or +6.8% relative to a

27   paired simulation without BC deposition. We also provide linear equations that

28   relate the increase in total runoff to GrIS-wide wet and dry BC deposition fluxes. It

29   is our hope that the runoff kernel and simple equations provided here can be used

30   to extend the utility of state-of-the-art aerosol models.

Atmospheric
Chemistry
and Physics
Discussions

1   Introduction

31

32   The Greenland Ice Sheet (GrIS) holds the equivalent of about 7 m of sea level

33   rise (Kintisch, 2017). During recent decades, the accelerating decline of the GrIS has

34   doubled Greenland's contribution to global sea level rise to about 0.74 mm per year

35   (Shepherd et al., 2012; Rignot and Kanagaratnam, 2006; van den Broeke et al., 2009;

36   Kintisch, 2017). Mass loss from the GrIS is predicted to raise sea level by more than

37   20 cm by 2100 (Rignot et al., 2011; Dumont et al., 2014), imposing tremendous

38   effects on global society.

39   Ice loss from the GrIS is caused by many physical and biological factors,

40   including: 1) increase of air temperature over the Arctic region, which accelerates

41   surface melting; 2) declining surface albedo, which can be caused by a variety of

42   effects including increased melt area, enhanced snow metamorphism, and

43   accumulation of light-absorbing impurities (LAI) (Tedesco et al., 2016; Box et al.,

44   2012; Dumont et al., 2014; Keegan et al., 2014; Shimada et al., 2016; Polashenski et

45   al., 2015); and 3) calving of icebergs and submarine melting due to ice dynamics and

46   changes of ocean temperature (Krabill et al., 2004; Zwally et al., 2002; Dumont et al.,

47   2014). Since 2005, surface melting has likely contributed more to ice loss than

48   iceberg calving (Kintisch, 2017). Sources of LAI include black carbon (BC), mineral

49   dust, and algae and bacteria growing on the wet surface of the ice sheet, all of which

50   darken the surface, boost the absorption of insolation and enhance snow melt.

51   BC is a major anthropogenic pollutant originating from fossil fuel combustion,

52   open biomass burning, and biofuel use, and is a key LAI because its solar

53 absorptivity is extremely high (e.g., Bond et al., 2013). Previous climate modeling

54 studies simulate annual warming in the Arctic region with the inclusion of BC in

55 snow (Flanner et al., 2007; Flanner et al., 2009; Hansen and Nazarenko, 2004;

56 Hansen et al., 2005; Jacobson, 2004), and find BC/snow forcing induces a global

57 temperature response about three times greater than equal forcing from CO_2

58 (Flanner et al., 2007). BC influences snow coverage by warming the atmosphere,

59 reducing surface insolation through "dimming", and reducing snow reflectance

60 through darkening caused by BC deposition to snow surface. Globally, the darkening

61 effect within snow increases solar heating of snowpack, and exceeds the loss of

62 absorbed energy from dimming, causing a positive net surface forcing and

63 snowpack melting (Flanner et al., 2009). Melting snow also tends to retain BC

64 aerosols, which darken the surface more and increase absorption of insolation (e.g.,

65 Doherty et al., 2013). Therefore, it is important for coupled aerosol-climate and ice

66 sheet models to include BC darkening effects, and yet most do not.

67   Global BC emissions from fossil fuel and biofuel combustion have increased

68 dramatically during the industrial era. Since the early 20th century, BC emissions

69 also shifted spatially, decreasing in North American and Europe but increasing in

70 Asia (Bond et al., 2007; Bond et al., 2013). Both the spatial pattern of emissions and

71 the circulation features that are coincident with emissions can strongly effect the

72 amount of BC reaching the Arctic and depositing to the GrIS (Doherty et al., 2010;

73 Thomas et al., 2017; Jiao et al., 2014).

74   In this study, we develop a BC deposition-snow melt kernel using the

75 Community Earth System Model (CESM) to investigate changes in snow melt and

76   surface runoff due to variations in the amount and timing of aerosol deposition on

77   the GrIS. More than 5000 simulations are conducted with the Community Land

78   Model (CLM) component of CESM, driven with a large range of wet and dry BC

79   deposition fluxes to determine relationships between snow melt perturbation and

80   deposition amount occurring in different months. The final kernel product is

81   resolved by type of BC deposition (wet or dry), deposition amount, deposition

82   month, and deposition year ranging from 2006-2015. It is our hope that this kernel

83   will benefit regional and global aerosol modeling communities by allowing them to

84   estimate GrIS snow melt and surface runoff perturbations associated with different

85   aerosol deposition fluxes.

86   **2   Methods**

87   **2.1   Simulation design**

88   We use the Community Earth System Model (CESM) version 1.2.2, and run the

89   offline Community Land Model (CLM) (Oleson et al., 2013) version 4.5 with

90   prescribed wet or dry BC deposition in the snow sub-model to study the effects of

91   BC deposition on snow melt and runoff from Greenland. Our motivation for using

92   CLM in this offline configuration is that (1) it reduces noise associated with ocean

93   and atmosphere variability, enabling clearer identification of the runoff signal

94   caused by snow perturbations, and (2) the simulations are computationally cheap,

95   allowing us to explore a large parameter space. We drive the simulations using

96   meteorological forcing data from the Climatic Research Unit and National Centers

97   for Environmental Prediction (CRUNCEP) (Viovy, 2012) over the period 2006-2016.

Atmospheric
Chemistry
and Physics
Discussions

98   CRUNCEP data cover the global land surface at a spatial resolution of a $0.5° \times 0.5°$,

99   and are provided with relatively low latency, allowing us to explore conditions over

100   the recent past. In CLM, the representation of terrestrial snow, including over ice

101   sheets, is based loosely on the SNTHERM model (Jordan, 1991) and is described in

102   detail by Oleson et al., 2013. Snow albedo and solar absorption within each snow

103   layer are simulated with the Snow, Ice, and Aerosol Radiative Model (SNICAR),

104   which accounts for solar zenith angle, albedo of the substrate underlying snow,

105   mass concentrations of LAI (black carbon, dust, organic carbon, and volcanic ash),

106   and ice effective grain size. In general, CLM/SNICAR represents five vertical snow

107   layers, and accounts for variations in LAI concentration due to dry and wet

108   deposition, particle flushing and retention with melt water, snow sublimation, and

109   layer combinations and divisions (Oleson et al., 2013). Dry BC deposition from the

110   atmosphere occurs through gravitational settling and turbulent mixing, primarily

111   transferring hydrophobic BC to the surface, while wet BC deposition occurs via

112   precipitation and only affects hydrophilic BC in the model. CLM maintains mass

113   burdens of both hydrophilic BC and hydrophobic BC within each snow layer, with

114   each species having unique optical properties and meltwater removal efficiencies.

115   Deposited particles are assumed to be instantly mixed and homogeneous within the

116   surface snow layer, which does not exceed 2cm in thickness. The particles are added

117   after the computation of inter-layer water fluxes, thus preventing particles in the

118   top layer from being washed out immediately before radiative calculations. Particle

119   masses are redistributed vertically in each time step proportionately with snow

120   melt through the snow column, scaled by the species-specific melt scavenging

Atmospheric
Chemistry
and Physics
Discussions

121   efficiency, and snow layer combination and subdivision. The masses carried out

122   with meltwater drainage through the bottom snow layer are permanently lost from

123   the snowpack, and are not maintained within the model (Oleson et al., 2013).

124   For each simulation used to generate the kernel relating melt runoff to BC

125   deposition, we prescribe uniform concentrations of BC within precipitation or

126   uniform dry deposition fluxes over the ice sheet for a period of one month, and

127   quantify perturbations to snow and melt runoff for one year or more following the

128   period of deposition. 23 unique BC concentrations in precipitation (e.g., snow) are

129   prescribed to provide wet BC flux in the CLM. We use a wide range of wet BC

130   concentrations (from 1 ng g^{-1} ~ 500 ng g^{-1}) with logarithmic spacing, aiming to

131   cover historically observed BC concentrations over the Greenland region (Figure 1)

132   and potential severe episodes associated (e.g.,) with extreme fire activity. For

133   example, measured values of BC in Greenland snow during 2012-2014, collected

134   from snow pits across a long transect, averaged 2.6 ng g^{-1} (Polashenski et al.,

135   2015). Peak values throughout the depth of the snow pits averaged 4 ng g^{-1} and 15

136   ng g^{-1} in 2012 and 2013, respectively, and the largest single measurement was 43 ng

137   g^{-1}. Ice core measurements from D4 dating back to 1788 show annual-mean

138   concentrations peaking in the early 20th century at ~12.5 ng g^{-1}, mean

139   concentrations of 2.3 ng g^{-1} during 1952-2002, and occasional monthly-mean peaks

140   exceeding 50 ng g^{-1} due to biomass burning events (McConnell et al., 2007).

141   Correspondingly, the maximum dry BC deposition flux is calculated as the product

142   of the maximum wet BC concentration (500 ng g^{-1}) and the mean monthly snowfall

143   (1.75×10^{-5} mm s^{-1}) over an 11-year (2006-2016) CESM simulation. We prescribe 24

144   unique dry BC fluxes (0.01 ng m^{-2} s^{-1}-8.80 ng m^{-2} s^{-1}) with logarithmic spacing in our

145   study (Figure 1).

146   With each prescribed BC deposition value, we perform 12 simulations with

147   specified BC deposition month from January to December in each deposition year.

148   Each simulation starts from January in the deposition year, and extends to one full

149   year after the deposition month in order to study the annually integrated BC effects.

150   We then repeat these simulations for ten years (2006-2015) to generate a

151   climatological product and explore the magnitude of interannual variability in melt

152   perturbations due, for example, to differences in precipitation and near-surface air

153   temperatures. In summary, we perform 2,760 simulations (23 wet BC

154   concentrations × 12 deposition months × 10 deposition years) to study the effects of

155   wet BC deposition, and 2,880 simulations (24 dry BC fluxes × 12 deposition months

156   × 10 deposition years) to study the effects of dry BC deposition. 120 simulations (12

157   deposition months × 10 deposition years) without BC deposition are also performed

158   as parallel control/base runs from which to derive the perturbations induced by BC

159   deposition.

160   **2.2   Simulation length evaluation based on top-snow layer BC concentration**

161   To evaluate the importance of simulation length for the purposes outlined, we

162   focus on BC concentration in the top snow layer because properties of this layer

163   dominate the bulk solar radiative properties of the snowpack. In Figure 2, we

164   examine the mean distribution of BC concentration in the top snow layer over

165   Greenland after maximum wet and dry BC deposition fluxes occur in January and

166   June. These contours are averaged over ten years to show a climatological state.

Atmospheric
Chemistry
and Physics
Discussions

Open Access

EGU

167   Top-layer BC concentrations after wet BC deposition show higher values in the

168   center and south margin of Greenland (Figure 2a, b, e, f), which matches the general

169   precipitation pattern over the GrIS, with elevated precipitation amount in the center

170   and south of GrIS. Meanwhile, higher top-layer BC values occur over the north of

171   Greenland after dry BC deposition (Figure 2c, d, g, h), as lower precipitation in these

172   regions enhances the effect of dry deposition. Also, we find lower concentrations

173   induced by the maximum wet BC (Figure 2a, b, e, f) than by the maximum dry BC

174   deposition (Figure 2c, d, g, h). Top-layer BC concentration decreases rapidly only

175   one month after the deposition month for both winter and summer deposition (i.e.,

176   from January to February with January deposition in Figure 2a-d, and from June to

177   July with June deposition in Figure 2e-h), as new snowfall dilutes the contaminated

178   snow. The rapid decrease in BC concentration supports the notion that a one-year

179   simulation length should capture most of the time-integrated effect from a

180   deposition event. To verify this, we also perform two 11-year (2006-2016)

181   simulations with the maximum wet BC deposition occurring in April and October of

182   the first year, to evaluate the long-term variation of top-layer BC concentration. In

183   these long-term simulations, we find top-layer BC concentrations decrease rapidly

184   within a one-year period after both spring and fall depositions (Figure 3). We also

185   see, however, that residual BC reappears at the surface in subsequent summers

186   because of snow melting and associated accumulation of impurities at the top of the

187   snowpack (Doherty et al., 2013). In the model, this occurs because melt scavenging

188   ratios for both types of BC are less than 1, meaning that proportionately less BC

189   moves down vertically in the column than meltwater. As we will see, summer re-

Atmospheric
Chemistry
and Physics
Discussions

190   appearance of impurities at the snow top has a non-negligible impact on the

191   annually-integrated runoff perturbation, but the peaks in subsequent years are less

192   than 1/20 of the BC concentrations in the deposition month, indicating that the one-

193   year simulation setup is reasonable to capture the major portion of the total BC

194   influences.

195   **3   Results and Discussion**

196   Deposited BC to snow causes a darkening effect and enhances snow melt and

197   Greenland runoff. Here, we first show variations of top-snow layer BC

198   concentrations, and then examine total GrIS runoff perturbation induced by BC

199   deposition.

200   **3.1   BC concentration in the top snow layer**

201   We investigate the climatological (i.e., averaged over ten simulations covering

202   2006-2015) 1-year evolution of top-snow layer BC concentration averaged over

203   Greenland for different deposition months. Figure 4 depicts the temporal evolution

204   of top-layer BC concentration for the maximum wet and dry BC fluxes from our

205   matrix of simulations. For all months of deposition, top-layer concentrations

206   decrease rapidly as fresh snow covers the contaminated surface. Top-snow layer

207   concentrations of dry-deposited BC generally decrease more slowly than those of

208   wet-deposited BC. One reason for this behavior during summer months is that dry-

209   deposited BC is assumed to be hydrophobic and have a lower meltwater scavenging

210   efficiency, reducing the rate at which it is carried away by melting water. We also

211   see, however, that some winter-deposited BC can persist in the top layer until, or

Atmospheric
Chemistry
and Physics
Discussions

212   even re-appear during, the summer melt season, indicating that BC deposition in

213   non-melting seasons can also be important for GrIS melting. Re-exposure of

214   previously deposited BC occurs as overlying snow melts and flushes through the

215   snow, removing some but not all of the underlying impurities and eventually

216   exposing the dirty snow layer at the surface.

217   We also investigate how top-layer BC concentration varies with different BC

218   deposition values, and how this variation evolves over one year following

219   deposition (Figure 5 and Figure 6). For all deposition months, top-snow layer BC

220   concentration increases, as expected, with increasing BC deposition flux. The

221   relationship between top-layer BC concentration and BC deposition value is nearly

222   linear, although we find indications of saturation at later times with dry BC

223   deposition (e.g., as in Figure 6h-l). Figure 7 summarizes top-layer BC concentration

224   variation with deposition amount at different times (0-11 months since deposition)

225   averaged over all the deposition months. With this averaging, we find that top-layer

226   BC concentrations decrease monotonically from month 0 to month 11. Again, we

227   find slower decrease in the dry deposition simulations than in the wet deposition

228   simulations. With wet BC deposition, the rate of decrease slows down after 3-6

229   months, which could be due to the summer peaks resulting from snow melting and

230   BC integration (Figure 4).

231   **3.2   Temporal variation of GrIS total runoff**

232   We define total runoff in CLM as the summation of surface runoff, sub-surface

233   drainage and runoff from glacier surface. We first examine the seasonal and inter-

234   annual variation of GrIS total runoff, integrated over the entire GrIS, in the base run

235   without BC deposition (Figure 8). Total runoff shows clear summer peaks and some

236   inter-annual variation. Annual-integrated total runoff is ~120 Gt per year, with the

237   highest value of ~140 Gt in 2014 (Figure 8b). Compared with satellite gravity

238   measurements during 2005-2010 showing Greenland is losing mass at a rate of

239   ~229 Gt/yr (169-290 Gt/yr), of which 50-70% is lost through surface melt

240   (Vaughan et al., 2013), the simulated total runoff in the base run in our study is

241   within a reasonable range.

242   We then calculate perturbed total runoff due to BC deposition as the difference

243   in runoff between simulations with BC deposition and paired base simulations

244   without BC deposition. We select three wet BC deposition values and three dry BC

245   deposition values to illustrate the seasonal and inter-annual variations of perturbed

246   total runoff (Figure 9). We note that different scales are used in the panels of Figure

247   9, which shows that higher deposition causes more total runoff. We also find clear

248   inter-annual variations for different deposition amounts and months. The variations

249   of perturbed total runoff in Figure 9 follow the variation of total runoff in the base

250   run (Figure 8) in general, especially for the perturbed simulations with wet BC

251   depositions, indicating that BC deposition could have greater effect in warmer years,

252   when more of the ice sheet is near the melting temperature.

253   To remove the effect of yearly variation, we also investigate the climatological

254   (i.e., averaged over ten simulations spanning 2006-2015) 1-year evolution of total

255   runoff increase due to BC deposition starting from different deposition months.

256   Again, we examine total runoff increase induced by maximum wet and dry BC

257   depositions to understand general behavior associated with very large

258   perturbations, for which the signal is much larger than noise. As shown in Figure

259   10, we find two summer peaks of total runoff increase, with the second peak caused

260   by the re-exposure of BC during the summer after deposition. We also find total

261   runoff perturbation is the largest in July for all months of deposition, followed by

262   August, due to higher temperature in summer.

263   **3.3   GrIS total runoff variation with deposition amount**

264   As represented by Figure 9, higher deposition amount causes larger total runoff

265   increase. Here, we examine total runoff perturbation caused by all deposition

266   amounts, and how total runoff distributes over Greenland. Figure 11 and Figure 12

267   show climatological mean (2006-2015) annually integrated total runoff increase

268   caused by June BC deposition via wet and dry processes, respectively. June

269   deposition is selected for these figures because of its high potential to impact

270   summer melt. Although BC is well distributed over the whole GrIS (Figure 2), total

271   runoff perturbations are largely confined to the low elevation margins with both

272   wet and dry BC deposition (Figure 11 and Figure 12), as these remain the only areas

273   warm enough in the model simulations for substantial melt to occur, which is

274   consistent with the Tedesco, 2007 study. We note that the spatial distribution of

275   model melt will be sensitive to surface air temperature and insolation, the latter of

276   which can vary substantially between re-analysis products. Runoff effects of dry BC

277   deposition show similar patterns as impacts from BC in precipitation. We find that

278   small fluxes of BC via dry deposition are not as effective as similar deposition fluxes

279   of BC in precipitation, and we attribute this to the higher light absorptivity (and

280   hence radiative forcing per unit mass) of hydrophilic BC than of hydrophobic BC.

13

Atmospheric
Chemistry
and Physics
Discussions
Open Access
EGU

281   The former is assumed to be coated with weakly-absorbing sulfate and hence its

282   mass absorption cross-section is about 50% larger than that of uncoated

283   hydrophobic BC (Flanner et al., 2007).

284   Figure 13 summarizes the variation of total runoff perturbation versus

285   deposition amount for different deposition months. The maximum BC deposition

286   perturbs total runoff by up to ~20% (24 Gt) in the wet BC deposition simulations,

287   although we note that continent-wide fluxes of this magnitude (500 ng g^{-1} in

288   precipitation) are much larger than ever observed on Greenland. With a modest

289   deposition concentration (e.g., 5 ng/g), the runoff perturbation is ~0.4% (~0.5 Gt).

290   Different deposition months cause annually integrated total runoff perturbation to

291   vary by 40-60% (12 Gt/yr in the maximum BC deposition case). Also, we find BC

292   deposition in June and July induces the largest annually integrated total runoff

293   increase. To further verify the most influential deposition month, we select five wet

294   BC and five dry BC deposition values, and plot total runoff increase versus

295   deposition month, shown in Figure 14. Figure 14a shows annual integrated total

296   runoff from the base run, starting from different months, serving as a reference for

297   the perturbations shown in Figure 14b-f. For different deposition amounts from low

298   to high (Figure 14b-f), BC deposition in summer (i.e., June, July and August) causes

299   the highest annual total runoff increase. With higher deposition (Figure 14e-f), June

300   deposition generates the largest annual total runoff for both dry and wet BC

301   deposition, whereas with lower deposition amounts the month of maximum impact

302   can be June or July. As noted earlier, however, deposition during non-summer

303   months also causes substantial melt and runoff perturbations, owing to the melt-

Atmospheric
Chemistry
and Physics
Discussions

Open Access

EGU

304   induced re-surfacing of impurities during summer in the ablation zone.

4   Evaluation and application of the kernel product

306   We turn now to evaluating the kernel product and advising a straightforward

307   way in which it can be applied to realistic aerosol deposition fluxes. We perform ten

308   one-year CLM simulations with spatially and temporally-varying wet or dry BC

309   deposition fluxes occurring in randomly selected years and months, and we evaluate

310   the accuracy of the kernel product using total GrIS BC deposition amount and total

311   runoff from these new simulations (the "evaluating simulations"), compared with

312   total runoff from the kernel for equivalent deposition fluxes. The evaluating

313   simulations use prescribed wet and dry BC deposition fields that were generated

314   from a global aerosol run with CAM (Lamarque et al., 2010). In different evaluating

315   simulations, the prescribed BC deposition fields are multiplied by factors ranging

316   from 2-50 for wet BC deposition and 2000-20000 for dry BC deposition to provide

317   different BC deposition amounts within the range of wet or dry deposition in the

318   kernel. High scaling factors are applied to dry/hydrophobic BC deposition

319   simulations because the prescribed dry BC deposition from CAM is very low and

320   within the noise regime. We also perform two ten-year (2006-2015) evaluating

321   simulations with both CAM prescribed wet and dry BC deposition fluxes turned on

322   throughout the whole simulations, to examine short-term, long-term and

323   climatological one-year integrated total runoff effects. BC deposition fluxes in one of

324   the ten-year evaluating simulations are multiplied by a factor of 5 to provide a high

325   deposition event and are left at unperturbed (i.e., realistic) values in the other

326   simulation. Also, different deposition years and months indicate different BC

327   distributions. Therefore, the evaluating simulations provide a variety of scenarios

328   with distinct BC deposition amounts and distributions to evaluate performance of

329   the kernel.

330   Figure 15 shows maximum, mean and minimum one-year integrated total

331   runoff increase versus BC deposition amount from the kernel product, with results

332   from the evaluating simulations overlaid on the kernel lines. With varying BC

333   deposition amount and distribution, including with combined wet and dry BC

334   deposition fluxes, results from the evaluating simulations are mostly within the total

335   runoff ranges of our kernel product for both wet and dry BC deposition. In the

336   evaluating simulations with combined wet and dry BC depositions, hydrophobic BC

337   fluxes are very low (<1/100 of wet BC fluxes), therefore, we treat all BC deposition

338   as wet/hydrophilic BC, and overlay the results on the wet deposition curves. We

339   note CAM simulated BC deposition from the 1 time evaluating run is comparable

340   with measured values of BC in Greenland snow and ice core measurements

341   (Polashenski et al., 2015; McConnell et al., 2007). The increases of one-year

342   integrated total runoff from the ten-year evaluating simulations with realistic

343   deposition exhibit wide ranges, for example, with a minimum of ~4 Gt in the first

344   deposition year (2006) to a maximum of ~10 Gt, and with a minimum of ~14 Gt in

345   the first year to a maximum of ~40 Gt in the simulation with 5 times BC fluxes. The

346   climatological (i.e., averaged over 10 years) total runoff perturbations (~8 Gt/yr and

347   ~30 Gt/yr in the default and 5 times simulations, respectively) caused by prescribed

348   combined wet and dry BC deposition are about double the first-year total runoff

349   integrations, which is due to continuous month by month depositions in the ten-

350   year evaluating simulations and the long-term effects of the reappearance of

351   residual BC at the surface as described in section 2.2.

352   Because the mean and maximum kernel curves in Figure 15 provide estimates

353   of BC induced total runoff within a reasonable range, we parameterize these curves

354   to provide a simple application of our kernel product. GrIS-wide melt perturbations

355   are relatively linear with BC deposition amount, with linear fits to the mean kernel

356   curves for wet and dry BC deposition fluxes of, respectively:

357   ΔTOTALRUNOFF = 4.498e5 * ΔwetBC,   (1)

358   ΔTOTALRUNOFF = 3.062e5 * ΔdryBC,   (2)

359   and with linear fits to the maximum kernel curves of:

360   ΔTOTALRUNOFF_MAX = 9.322e5 * ΔwetBC,   (3)

361   ΔTOTALRUNOFF_MAX = 6.348e5 * ΔdryBC,   (4)

362   where ΔTOTALRUNOFF is the mean increase in one-year integrated total runoff (kg

363   yr^{-1}), ΔTOTALRUNOFF_MAX is the maximum increase in one-year integrated total

364   runoff (kg yr^{-1}), and ΔwetBC and ΔdryBC are total wet and dry BC deposition fluxes

365   to the GrIS (kg yr^{-1}). Unique relationships for wet and dry deposition arise, again,

366   because of differences in optical properties and melt-induced removal efficiencies of

367   hydrophilic and hydrophobic BC. Linearity in the relationship between runoff and

368   BC deposition is encouraging because we have neglected coincident darkening from

369   other types of LAI (e.g., dust, algae). In environments where darkening from other

370   LAI is not too great, the runoff–BC relationships derived here should be valid,

371   though we acknowledge that the incremental effect of BC will be lower in snow that

Atmospheric
Chemistry
and Physics
Discussions

372   is heavily laden with other impurities.

373   The bulk relationships shown above represent the simplest application of our

374   kernel product, allowing a rough estimation of runoff perturbation caused by

375   Greenland-wide wet and dry BC deposition fluxes. Based on the evaluations in

376   Figure 15, the mean curves (i.e., equations (1) and (2)) from the kernel product tend

377   to provide a conservative estimate of total runoff, whereas the maximum curves

378   (i.e., equations (3) and (4)) represent a more realistic approximation of total runoff

379   induced by BC deposition that occurs continuously and with varying spatial

380   distribution. Ideally, gridcell-by-gridcell fluxes should be matched to the kernel to

381   account for spatial differences in melt associated with elevation and other

382   conditions (Figure 11 and Figure 12), but at the low end of deposition flux we see

383   considerable noise at the individual pixel and deposition month level, especially for

384   wet deposition fluxes that can be subject to anomalies associated with low

385   precipitation amounts in a given month. To ameliorate this, for typical present-day

386   deposition fluxes we recommend matching month-specific, but spatially-integrated

387   deposition fluxes or concentrations with the associated Greenland-wide kernel

388   values.

389   Finally, although this product only includes BC, we suggest that it could be

390   extended to include other LAI species through a simple scaling that accounts for the

391   ratio of mass-specific absorption between the species of interest and the BC

392   explored here. Rationale for this is that radiative forcing and melt perturbation will

393   scale roughly linearly with absorptivity, at least for relatively low and moderate

394   burdens of LAI. The mass-specific visible band absorption cross-sections assumed

Atmospheric
Chemistry
and Physics
Discussions

395   in our study for hydrophilic (via wet deposition) and hydrophobic (via dry

396   deposition) BC are 7.5 and 11.3 $m^2\,g^{-1}$, respectively. The only other species-specific

397   property affecting results from this study is the meltwater scavenging coefficient,

398   which is assumed to be 0.2 for hydrophilic BC and 0.03 for hydrophobic BC (Flanner

399   et al., 2007). Given relatively large uncertainty in this parameter (Doherty et al.,

400   2013; Qian et al., 2014), we suggest applying the hydrophilic (wet deposition)

401   kernel to all hydrophilic species and the hydrophobic (dry deposition) kernel to all

402   hydrophobic species, along with appropriate scaling of optical properties.

403   **5   Conclusions**

404   In this study, ~6,000 simulations are performed to investigate annually

405   integrated runoff perturbation from BC deposition on snow. The simulation matrix

406   includes variations in deposition flux, deposition month and year, and nature of the

407   deposition (wet or dry). From this matrix we produce a large-ensemble kernel that

408   relates BC deposition fluxes to GrIS runoff perturbations.

409   In the month after deposition, top-snow layer BC concentration decreases

410   rapidly due to fresh snow coverage, but then increases somewhat in the ablation

411   zone during the following summer due to melt-induced re-exposure of the

412   contaminated snow. Accordingly, the total runoff increase induced by BC deposition

413   is substantial for both summer and winter deposition, though with peak impacts

414   associated with June and July deposition. Impacts from winter deposition suggest

415   that winter emissions, associated for example with biomass heating use, should not

416   be neglected as potential contributors to increased summer melt. Also, we find most

417   of the runoff increase occurs along the margins, and especially on the southern

418   margin of Greenland, with little sign of melting in the center of the GrIS where it is

419   rarely warm enough. Inter-annual variations in total runoff in the base and BC

420   perturbed simulations indicate that BC deposition can generate more impact in

421   warmer years, when more of the ice surface is near the melting temperature.

422   In summary, higher BC deposition amount leads to higher total runoff. We do

423   not find a clear sign of runoff saturation caused by high BC deposition values in our

424   study. Model-generated deposition fluxes associated with realistic BC emissions

425   induce a climatological-mean (2006-2015) GrIS-wide runoff increase of 8 Gt/yr

426   (+6.8% perturbation), which corresponds to 0.022 mm/year of global sea level rise.

427   We also suggest simple, linear equations that crudely relate GrIS-wide wet and dry

428   BC deposition fluxes to annually-integrated runoff perturbation, and provide links

429   to the full spatially-varying kernel dataset so that users can derive more accurate

430   estimates of melt perturbation (e.g., resolved by seasonal timing) from deposition

431   fluxes. We also suggest that the kernel results can be applied to other LAI species

432   via simple scaling of the mass absorption cross-section. Our hope is that these data

433   will extend the utility of state-of-the-art aerosol models.

434

Atmospheric
Chemistry
and Physics
Discussions

References

443 Bond, T. C., Bhardwaj, E., Dong, R., Jogani, R., Jung, S., Roden, C., Streets, D. G., and
444   Trautmann, N. M.: Historical emissions of black and organic carbon aerosol from
445   energy-related combustion, 1850–2000, Global Biogeochemical Cycles, 21, n/a-
446   n/a, 10.1029/2006GB002840, 2007.
447 Bond, T. C., Doherty, S. J., Fahey, D. W., Forster, P. M., Berntsen, T., DeAngelo, B. J.,
448   Flanner, M. G., Ghan, S., Kärcher, B., Koch, D., Kinne, S., Kondo, Y., Quinn, P. K.,
449   Sarofim, M. C., Schultz, M. G., Schulz, M., Venkataraman, C., Zhang, H., Zhang, S.,
450   Bellouin, N., Guttikunda, S. K., Hopke, P. K., Jacobson, M. Z., Kaiser, J. W., Klimont,
451   Z., Lohmann, U., Schwarz, J. P., Shindell, D., Storelvmo, T., Warren, S. G., and
452   Zender, C. S.: Bounding the role of black carbon in the climate system: A scientific
453   assessment, Journal of Geophysical Research: Atmospheres, 118, 5380-5552,
454   10.1002/jgrd.50171, 2013.
455 Box, J., Fettweis, X., Stroeve, J., Tedesco, M., Hall, D., and Steffen, K.: Greenland ice
456   sheet albedo feedback: thermodynamics and atmospheric drivers, The
457   Cryosphere, 6, 821-839, 2012.
458 Doherty, S., Warren, S., Grenfell, T., Clarke, A., and Brandt, R.: Light-absorbing
459   impurities in Arctic snow, Atmospheric Chemistry and Physics, 10, 11647-11680,
460   2010.
461 Doherty, S. J., Grenfell, T. C., Forsström, S., Hegg, D. L., Brandt, R. E., and Warren, S. G.:
462   Observed vertical redistribution of black carbon and other insoluble light‐
463   absorbing particles in melting snow, Journal of Geophysical Research:
464   Atmospheres, 118, 5553-5569, 2013.
465 Dumont, M., Brun, E., Picard, G., Michou, M., Libois, Q., Petit, J. R., Geyer, M., Morin, S.,
466   and Josse, B.: Contribution of light-absorbing impurities in snow to Greenland's
467   darkening since 2009, Nature Geoscience, 7, 509, 10.1038/ngeo2180
468   https://www.nature.com/articles/ngeo2180#supplementary-information, 2014.
469 Flanner, M. G., Zender, C. S., Randerson, J. T., and Rasch, P. J.: Present-day climate
470   forcing and response from black carbon in snow, Journal of Geophysical
471   Research: Atmospheres, 112, n/a-n/a, 10.1029/2006JD008003, 2007.
472 Flanner, M. G., Zender, C. S., Hess, P. G., Mahowald, N. M., Painter, T. H., Ramanathan,
473   V., and Rasch, P.: Springtime warming and reduced snow cover from
474   carbonaceous particles, Atmospheric Chemistry and Physics, 9, 2481-2497, 2009.
475 Hansen, J., and Nazarenko, L.: Soot climate forcing via snow and ice albedos,
476   Proceedings of the National Academy of Sciences of the United States of America,
477   101, 423-428, 2004.
478 Hansen, J. e., Sato, M., Ruedy, R., Nazarenko, L., Lacis, A., Schmidt, G., Russell, G.,
479   Aleinov, I., Bauer, M., and Bauer, S.: Efficacy of climate forcings, Journal of
480   Geophysical Research: Atmospheres, 110, 2005.

Atmospheric
Chemistry
and Physics
Discussions

481   Jacobson, M. Z.: Climate response of fossil fuel and biofuel soot, accounting for soot's
482   feedback to snow and sea ice albedo and emissivity, Journal of Geophysical
483   Research: Atmospheres, 109, 2004.
484   Jiao, C., Flanner, M., Balkanski, Y., Bauer, S., Bellouin, N., Berntsen, T., Bian, H.,
485   Carslaw, K., Chin, M., and De Luca, N.: An AeroCom assessment of black carbon in
486   Arctic snow and sea ice, Atmospheric Chemistry and Physics, 14, 2399-2417,
487   2014.
488   Jordan, R.: A one-dimensional temperature model for a snow cover: Technical
489   documentation for SNTHERM. 89, COLD REGIONS RESEARCH AND ENGINEERING
490   LAB HANOVER NH, 1991.
491   Keegan, K. M., Albert, M. R., McConnell, J. R., and Baker, I.: Climate change and forest
492   fires synergistically drive widespread melt events of the Greenland Ice Sheet,
493   Proceedings of the National Academy of Sciences, 111, 7964-7967, 2014.
494   Kintisch, E.: Meltdown, in, American Association for the Advancement of Science,
495   2017.
496   Krabill, W., Hanna, E., Huybrechts, P., Abdalati, W., Cappelen, J., Csatho, B., Frederick,
497   E., Manizade, S., Martin, C., and Sonntag, J.: Greenland ice sheet: increased coastal
498   thinning, Geophysical Research Letters, 31, 2004.
499   Lamarque, J.-F., Bond, T. C., Eyring, V., Granier, C., Heil, A., Klimont, Z., Lee, D.,
500   Liousse, C., Mieville, A., and Owen, B.: Historical (1850–2000) gridded
501   anthropogenic and biomass burning emissions of reactive gases and aerosols:
502   methodology and application, Atmospheric Chemistry and Physics, 10, 7017-
503   7039, 2010.
504   McConnell, J. R., Edwards, R., Kok, G. L., Flanner, M. G., Zender, C. S., Saltzman, E. S.,
505   Banta, J. R., Pasteris, D. R., Carter, M. M., and Kahl, J. D.: 20th-century industrial
506   black carbon emissions altered arctic climate forcing, Science, 317, 1381-1384,
507   2007.
508   Oleson, K., Lawrence, M., Bonan, B., Drewniak, B., Huang, M., Koven, D., Levis, S., Li, F.,
509   Riley, J., and Subin, M.: Technical description of version 4.5 of the Community
510   Land Model (CLM), 2013.
511   Polashenski, C. M., Dibb, J. E., Flanner, M. G., Chen, J. Y., Courville, Z. R., Lai, A. M.,
512   Schauer, J. J., Shafer, M. M., and Bergin, M.: Neither dust nor black carbon causing
513   apparent albedo decline in Greenland's dry snow zone: Implications for MODIS
514   C5 surface reflectance, Geophysical Research Letters, 42, 9319-9327, 2015.
515   Qian, Y., Wang, H., Zhang, R., Flanner, M. G., and Rasch, P. J.: A sensitivity study on
516   modeling black carbon in snow and its radiative forcing over the Arctic and
517   Northern China, Environmental Research Letters, 9, 064001, 2014.
518   Rignot, E., and Kanagaratnam, P.: Changes in the velocity structure of the Greenland
519   Ice Sheet, Science, 311, 986-990, 2006.
520   Rignot, E., Velicogna, I., van den Broeke, M. R., Monaghan, A., and Lenaerts, J. T.:
521   Acceleration of the contribution of the Greenland and Antarctic ice sheets to sea
522   level rise, Geophysical Research Letters, 38, 2011.
523   Shepherd, A., Ivins, E. R., Geruo, A., Barletta, V. R., Bentley, M. J., Bettadpur, S., Briggs,
524   K. H., Bromwich, D. H., Forsberg, R., and Galin, N.: A reconciled estimate of ice-
525   sheet mass balance, Science, 338, 1183-1189, 2012.

526 Shimada, R., Takeuchi, N., and Aoki, T.: Inter-annual and geographical variations in
527   the extent of bare ice and dark ice on the Greenland ice sheet derived from MODIS
528   satellite images, Frontiers in Earth Science, 4, 43, 2016.
529 Tedesco, M.: Snowmelt detection over the Greenland ice sheet from SSM/I
530   brightness temperature daily variations, Geophysical Research Letters, 34, 2007.
531 Tedesco, M., Doherty, S., Fettweis, X., Alexander, P., Jeyaratnam, J., and Stroeve, J.:
532   The darkening of the Greenland ice sheet: trends, drivers, and projections (1981–
533   2100), Cryosphere (The), 10, 477-496, 2016.
534 Thomas, J. L., Polashenski, C. M., Soja, A. J., Marelle, L., Casey, K., Choi, H. D., Raut, J. C.,
535   Wiedinmyer, C., Emmons, L. K., and Fast, J.: Quantifying black carbon deposition
536   over the Greenland ice sheet from forest fires in Canada, Geophysical Research
537   Letters, 2017.
538 van den Broeke, M., Bamber, J., Ettema, J., Rignot, E., Schrama, E., van de Berg, W. J.,
539   van Meijgaard, E., Velicogna, I., and Wouters, B.: Partitioning recent Greenland
540   mass loss, science, 326, 984-986, 2009.
541 Vaughan, D. G., Comiso, J. C., Allison, I., Carrasco, J., Kaser, G., Kwok, R., Mote, P.,
542   Murray, T., Paul, F., and Ren, J.: Observations: cryosphere, Climate change, 2103,
543   317-382, 2013.
544 Viovy, N.: CRU-NCEP Version 4, available at:
545   http://dods.extra.cea.fr/data/p529viov/cruncep/V4_1901_2012/ last access:
546   August 2012.
547 Zwally, H. J., Abdalati, W., Herring, T., Larson, K., Saba, J., and Steffen, K.: Surface
548   melt-induced acceleration of Greenland ice-sheet flow, Science, 297, 218-222,
549   2002.
550

551 **Figure Captions**

552
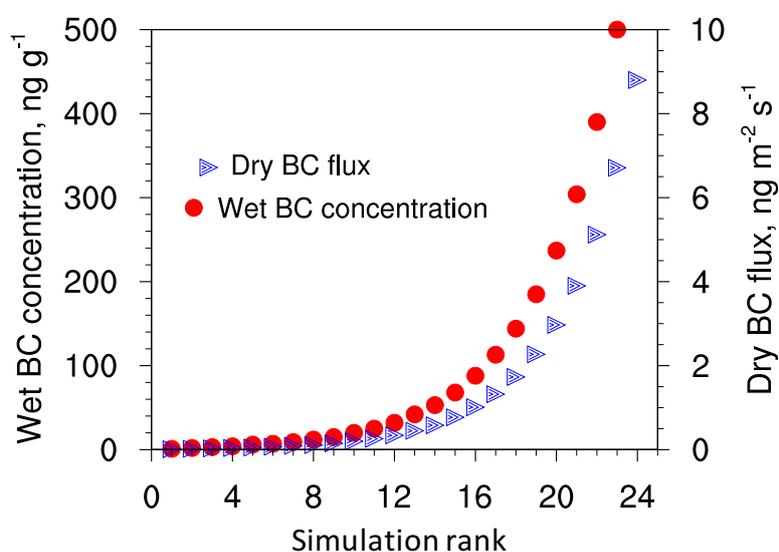
553

554 **Figure 1.** Prescribed values of BC concentrations in precipitation (red) and dry

555 deposition fluxes (blue) applied in the CESM modeling studies. Spacing between

556 values is logarithmic.

557

Atmospheric
Chemistry
and Physics
Discussions
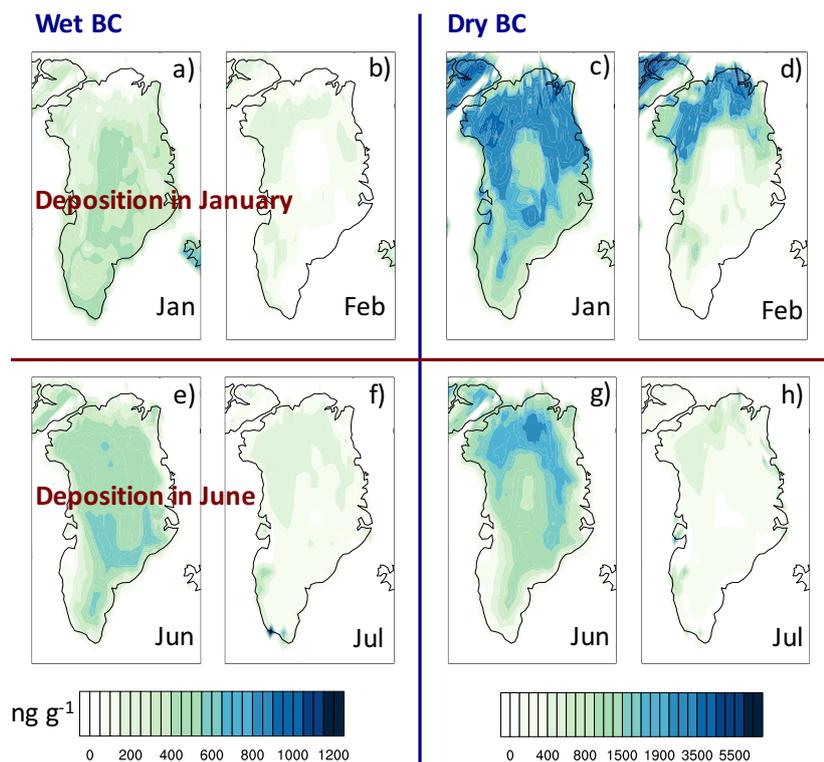
Figure 2. Ten-year (2006-2015) averaged hydrophilic BC concentration associated

with wet deposition (a, b, e, f) and hydrophobic BC concentration associated with

dry deposition (c, d, g, h) in the top snow layer. The contour maps show

concentrations caused by January deposition (a-d) and June deposition (e-h),

associated with the maximum wet and dry deposition scenarios depicted in Figure

1.

Atmospheric
Chemistry
and Physics
Discussions
Open Access
EGU

566
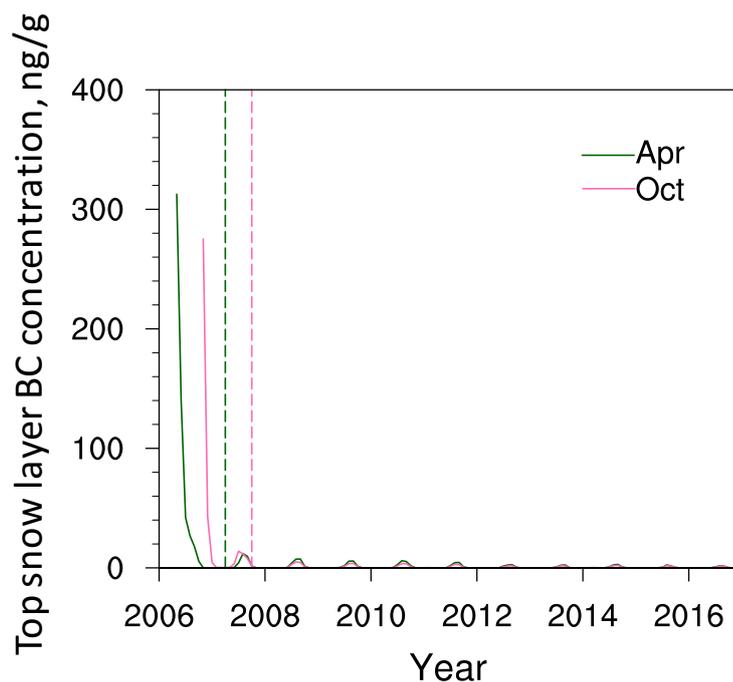
Figure 3. Temporal evolution of hydrophilic BC concentration in the top snow layer

averaged over the Greenland region from two 11-year (2006-2016) simulations

with wet BC deposition occurring in April and October of the first year. The BC

concentration in precipitation is the maximum value shown in Figure 1. Dashed

lines represent the ends of one year since different deposition months.

572

573
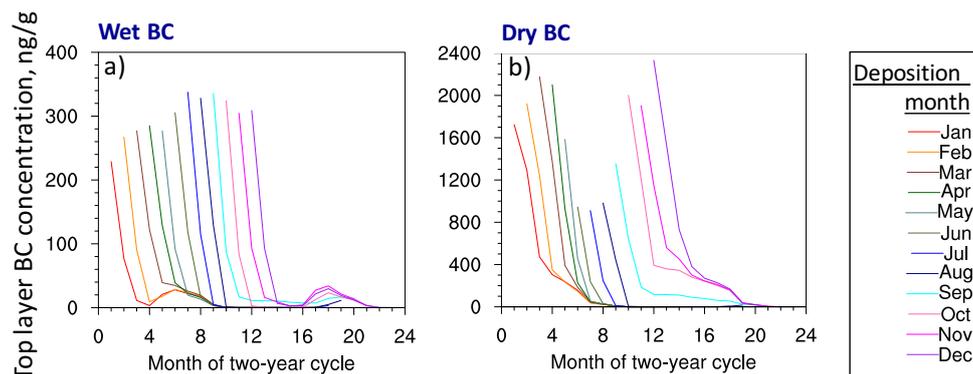
Figure 4. Temporal evolution of hydrophilic BC concentration (a) and hydrophobic

BC concentration (b) in the top snow layer averaged over the Greenland region from

the simulations with the maximum wet and dry BC deposition, respectively. Each

line starts from the BC deposition month, extends one year, and represents the

mean time series from 10 simulations that start in each year from 2006-2015.

579

Atmospheric
Chemistry
and Physics
Discussions

580
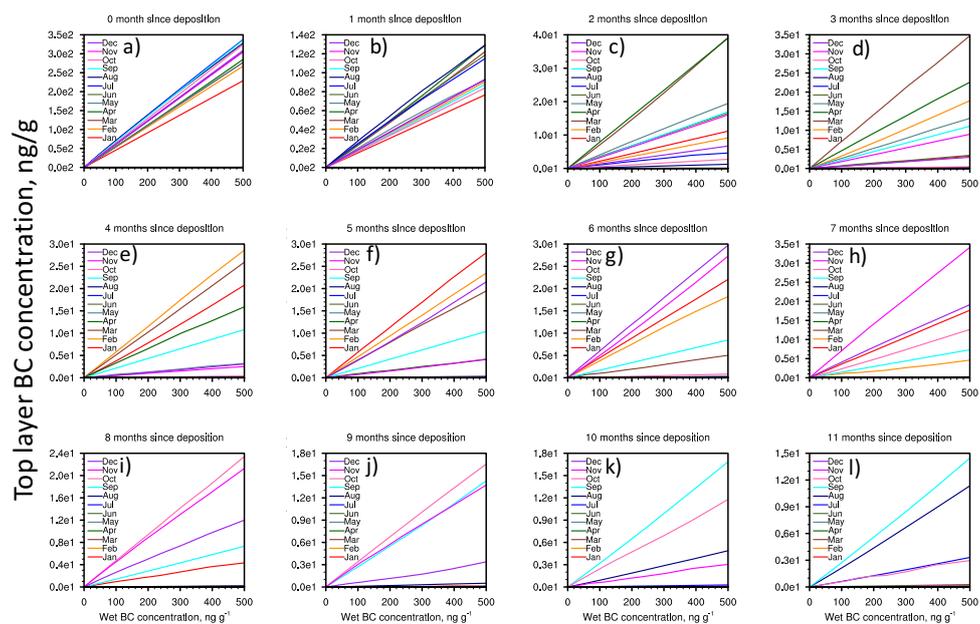
Figure 5. Hydrophilic BC concentration in the top snow layer vs. concentration of

BC in precipitation shown at different times (0-11 months, panels a-l) since

deposition. The top-snow layer concentrations are averaged over the Greenland

region and over ten one-year simulations beginning in years 2006-2015. Different

line colors represent different deposition months.

586

587
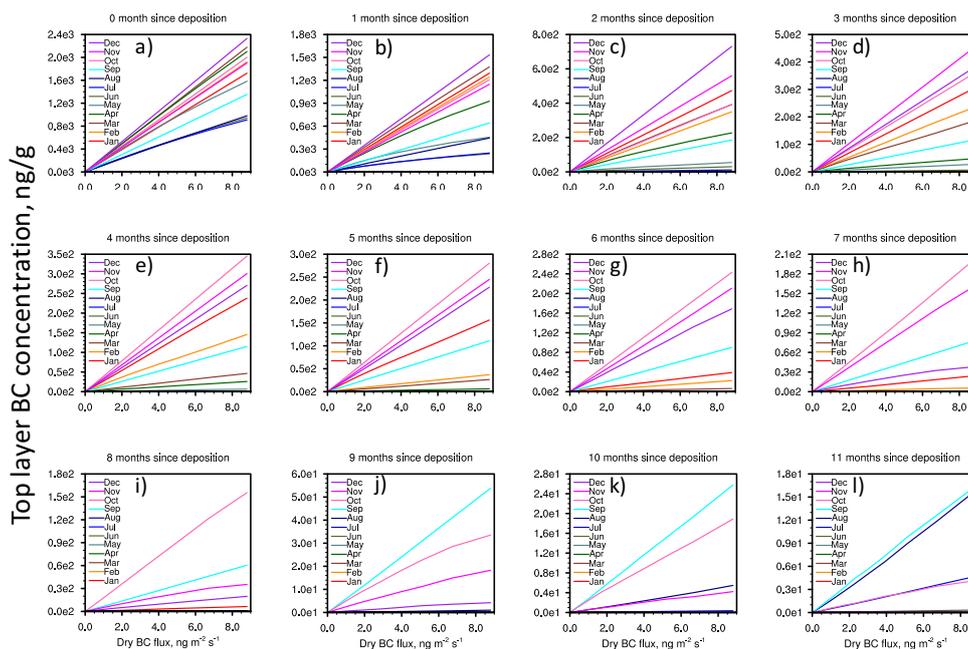
Figure 6. Same as Figure 5, but showing hydrophobic BC concentration in the top

snow layer vs. BC dry deposition flux.

590

591

592

593

594
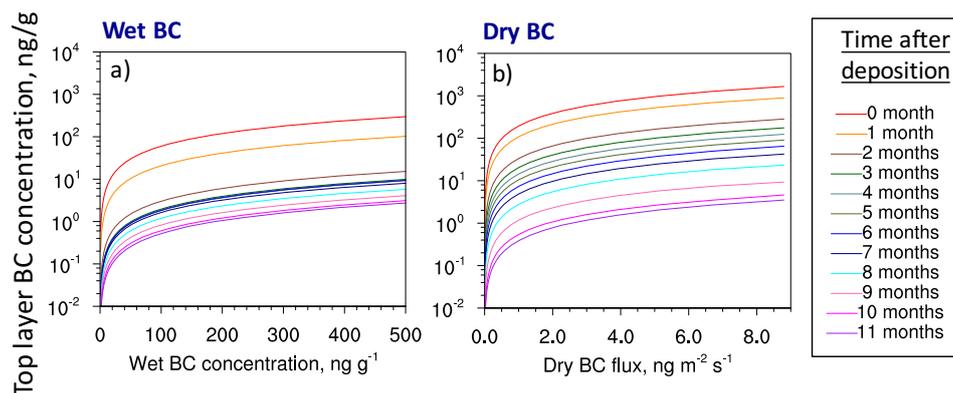
Figure 7. Hydrophilic BC concentration in the top snow layer vs. concentration of BC in precipitation (a), and hydrophobic BC concentration in the top snow layer vs. BC dry deposition flux (b) shown at different times (0-11 months) since deposition. The top-snow layer concentrations are averaged over the Greenland region, over all the deposition months and over ten one-year simulations beginning in years 2006-2015.

603
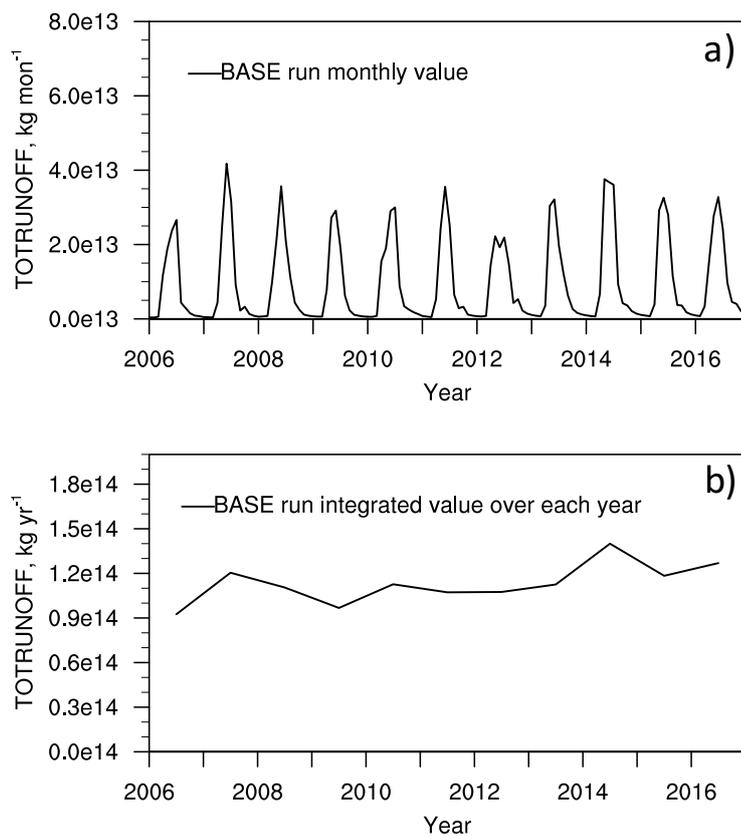
Figure 8. Monthly (a) and annually integrated (b) timeseries of total runoff from

Greenland in the Base run without BC deposition.

606
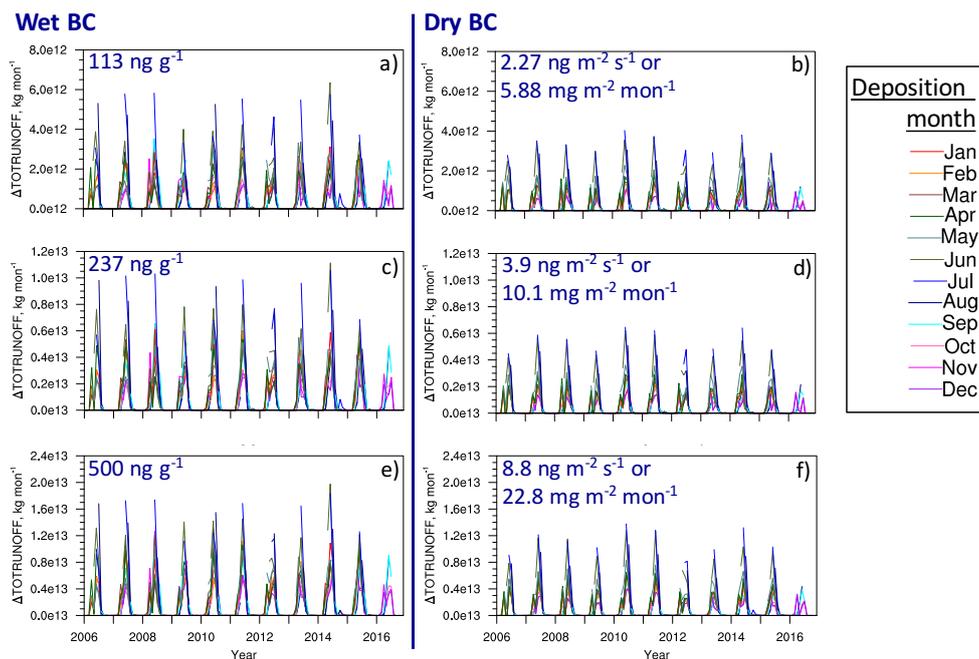
Figure 9. Monthly timeseries of the increase in total Greenland runoff resulting

from BC deposition. Values of BC concentrations in precipitation (a, c, e) and dry

deposition fluxes (b, d, f) are shown in each plot. Each line starts from the BC

deposition month and extends one year. Different line colors represent different

deposition months.
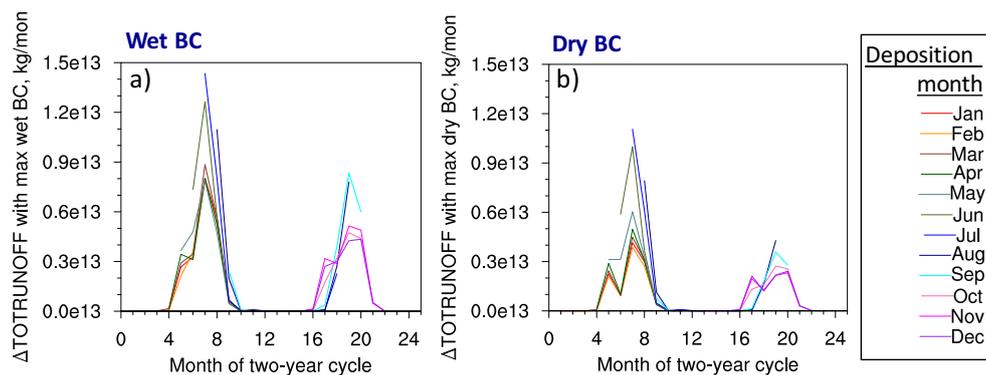
Figure 10. Temporal evolution of ten-year (2006-2015) averaged total runoff increase resulting from BC deposition, summed over the entire Greenland region from the simulations with the maximum wet (a) and dry (b) BC deposition. Each line starts from the BC deposition month and extends one year.
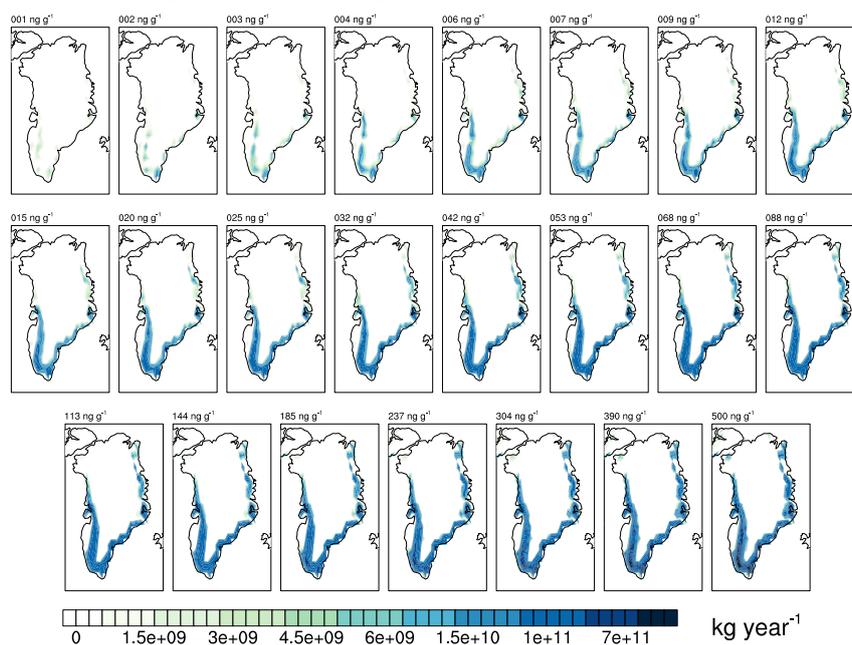
Figure 11. Ten-year average of annually-integrated total runoff increase resulting from different concentrations of BC in precipitation, deposited only during June. The average is over ten one-year simulations starting in each year from 2006-2015.

620

621

622

623

624
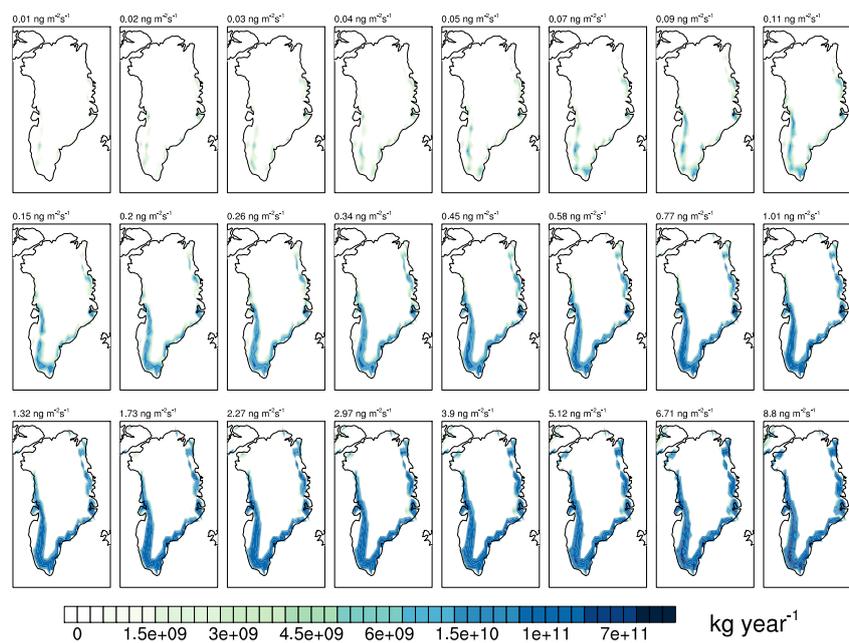
Figure 12. Same as Figure 11, but resulting from different dry deposition fluxes of BC in June.

Atmospheric
Chemistry
and Physics
Discussions

631
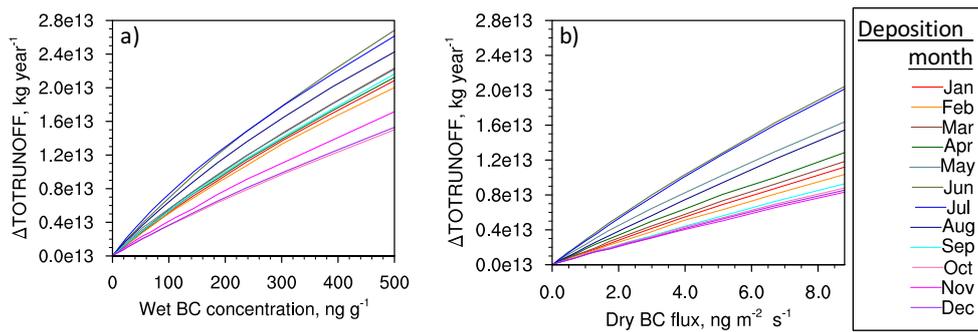
Figure 13. Increase in total Greenland runoff resulting from BC deposition

integrated over one year starting from the month of BC deposition vs. concentration

of BC in precipitation (a) and vs. BC dry deposition flux (b). The runoff values are

summed over the Greenland region and averaged over ten one-year simulations

beginning in years 2006-2015. Different line colors represent different deposition

months.

638

639

640
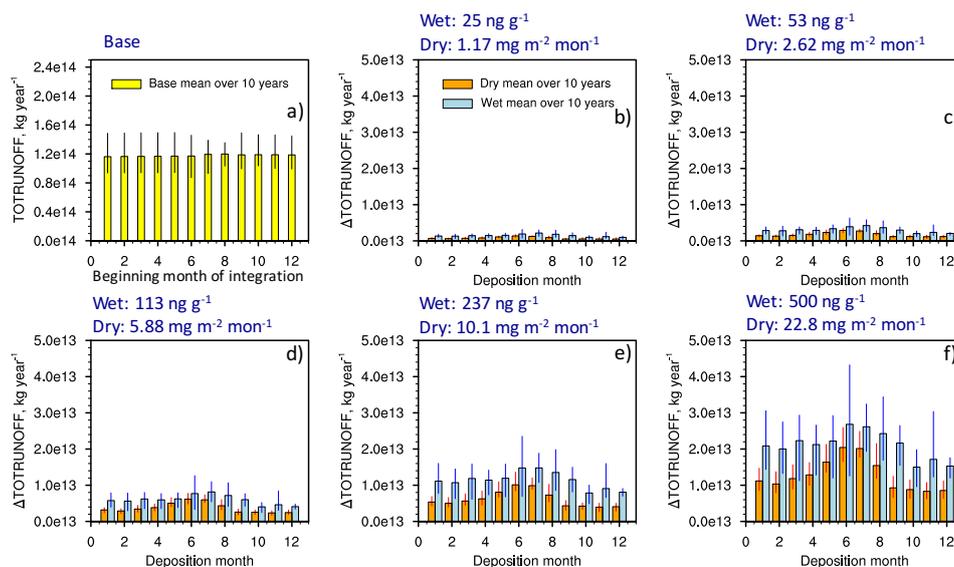
Figure 14. Total runoff in the Base run without BC deposition (a) and the increase

in total Greenland runoff resulting from BC deposition (b-f), integrated over one

year starting from the month of BC deposition. The bars show mean values and the

whiskers depict the full range of values over all ten simulations that each start in a

different year from 2005-2016. Values of BC concentrations in precipitation and dry

deposition fluxes are shown in the title of each plot (b-f).

647

648
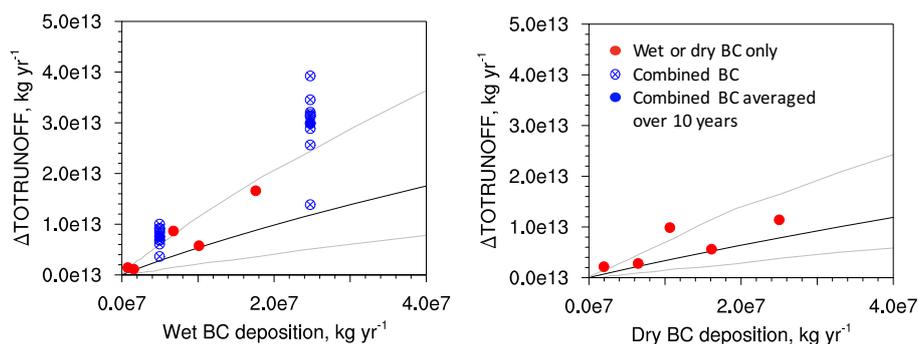
Figure 15. Increase in total Greenland runoff resulting from BC deposition

integrated over one year starting from the month of BC deposition vs. total wet (a)

and dry (b) BC deposition mass flux over the entire GrIS. The runoff values are

summed over the Greenland region and averaged over all deposition years and

deposition months. Black lines show mean total runoff values, and grey lines show

maximum and minimum values from the entire matrix of simulations. Red dots

represent explicitly-simulated total runoff from the evaluating simulations with

prescribed spatially and temporally-varying wet or dry BC deposition fluxes in

randomly selected months and years. Blue hollow circles represent simulated total

runoff from the evaluating simulations with prescribed combined BC deposition

fluxes integrated over each year of the ten-year simulations. Blue dots show

averages of the hollow circles.

661